

Vision-Language Model Based Multi-Expert Fusion for CT Image Classification

Jianfa Bai¹, Kejin Lu¹, Runtian Yuan¹, Qingqiu Li¹, Jilan Xu², Junlin Hou^{3*}, Yuejie Zhang^{1*}, Rui Feng^{1*}

¹College of Computer Science and Artificial Intelligence,
Shanghai Key Laboratory of Intelligent Information Processing, Fudan University

²University of Oxford

³The Hong Kong University of Science and Technology

Abstract

Robust detection of COVID-19 from chest CT remains challenging in multi-institutional settings due to substantial source shift, source imbalance, and hidden test-source identities. In this work, we propose a three-stage source-aware multi-expert framework for multi-source COVID-19 CT classification. First, we build a lung-aware 3D expert by combining original CT volumes and lung-extracted CT volumes for volumetric classification. Second, we develop two MedSigLIP-based experts: a slice-wise representation and probability learning module, and a Transformer-based inter-slice context modeling module for capturing cross-slice dependency. Third, we train a source classifier to predict the latent source identity of each test scan. By leveraging the predicted source information, we perform model fusion and voting based on different experts. On the validation set covering all four sources, the Stage 1 model achieves the best macro-F1 of 0.9711, ACC of 0.9712, and AUC of 0.9791. Stage 2a and Stage 2b achieve the best AUC scores of 0.9864 and 0.9854, respectively. Stage 3 source classifier reaches 0.9107 ACC and 0.9114 F1. These results demonstrate that source-aware expert modeling and hierarchical voting provide an effective solution for robust COVID-19 CT classification under heterogeneous multi-source conditions.

1. Introduction

Robust detection of COVID-19 from chest CT is not merely a classification problem, but a domain-generalization problem under substantial variation between institutions [1–5, 10–22, 25–28]. In multi-center clinical settings, CT scans may differ markedly in scanner vendors, reconstruction kernels, slice counts, field-of-view, and background artifacts, while patient populations and disease presentations also vary across hospitals. As a result, a model trained on one source can perform well in-distribution yet degrade noticeably on unseen or shifted sources. This issue becomes

even more critical in the Multi-Source COVID-19 Detection Challenge, where the task explicitly involves four distinct medical sources and therefore directly evaluates whether a method can maintain reliable performance under source shift rather than simply fit a single pooled dataset.

To address these limitations, we propose a **three-stage source-aware multi-expert framework** for multi-source COVID-19 CT classification. As illustrated in Fig. 1, Stage 1 builds a lung-aware 3D expert that performs lung extraction and unified volume canonicalization before 3D classification, reducing irrelevant peripheral background and preserving volumetric morphology. Stage 2 introduces two complementary 2D experts based on a pretrained MedSigLIP [23] encoder: Stage 2a performs slice-wise probability learning by randomly sampling contiguous slices during training and averaging per-slice predictions, while Stage 2b removes the original classification head and adds lightweight Transformer [24] encoder blocks to refine inter-slice context before classification. Stage 3 further trains a source classifier to estimate the latent source identity of each test scan and route samples to appropriate experts. To improve stability, we also train multiple model variants within each step and aggregate their outputs by voting.

Our framework is designed together with challenge-specific data handling. We first perform lung extraction for all scans and suppress excessive peripheral dark regions. We then apply a unified preprocessing rule that discards the first and last 15% of slices when the slice count exceeds 150, followed by stage-specific canonicalization for 3D and 2D pipelines. To alleviate the zero-positive validation issue of source 2, we include its 39 positive training cases in validation-oriented source analysis. We also correct the source 0 non-COVID training count based on folder-level inspection and predict test-source identities for source-aware inference. These steps are important for reliable model development under scarce and imperfect source supervision.

Extensive experiments validate the effectiveness of the proposed design. Stage 1 achieves a best macro-F1 of

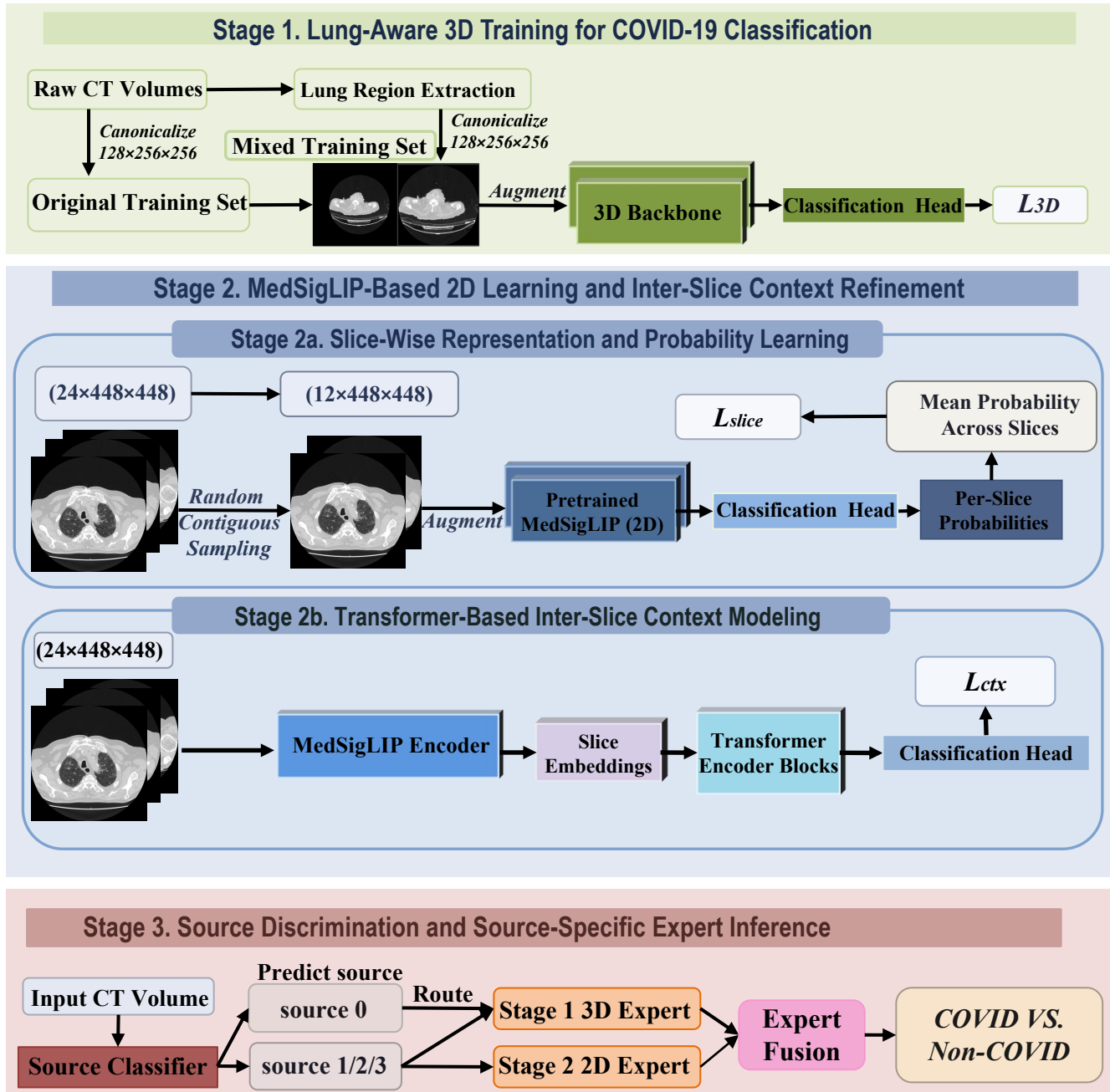


Figure 1. Overview of the proposed three-stage source-aware multi-expert framework for multi-source COVID-19 CT classification. Stage 1 builds a lung-aware 3D expert for volumetric classification. Stage 2 introduces two MedSigLIP-based 2D experts for slice-wise probability learning and inter-slice context modeling. Stage 3 performs source discrimination and source-specific expert inference, where source 0 is handled by the 3D expert and source 1/2/3 are jointly inferred by multiple experts through fusion and voting.

97.11%, AUC of 98.29%, and accuracy of 97.12%. Stage 2a reaches a best macro-F1 of 94.50%, AUC of 98.64%, and accuracy of 94.81%, while Stage 2b further improves to 95.82% macro-F1, 98.54% AUC, and 95.97% accuracy. The Stage 3 source classifier achieves 91.07% accuracy and 91.14% F1, providing a reliable basis for source-aware

routing. Notably, the Stage 1 3D expert attains perfect accuracy on source 0, which directly motivates our final source-specific expert allocation strategy.

Our main contributions are summarized as follows:

- We reformulate multi-source COVID-19 CT detection as a **source-aware domain-robust classification problem**

and explicitly address hidden test sources, source imbalance, and validation sparsity.

- We propose a **three-stage multi-expert framework** that combines a lung-aware 3D expert, two MedSigLIP-based 2D experts, and a source classifier for source-specific inference.
- We introduce a **hierarchical voting and fusion strategy** that integrates multiple models within each step and jointly exploits heterogeneous experts for source 1/2/3 prediction.
- We achieve strong validation performance across stages, with the best Stage 1 model reaching **97.10%** macro-F1, demonstrating the effectiveness of source-aware expert modeling for robust multi-source COVID-19 CT classification.

2. Methodology

2.1. Overview

As illustrated in Fig. 1, we propose a three-stage source-aware multi-expert framework for robust multi-source COVID-19 CT classification. Given a chest CT scan X with binary label $y \in \{0, 1\}$, where $y = 1$ denotes *COVID* and $y = 0$ denotes *Non-COVID*, our goal is to learn complementary experts under heterogeneous source distributions and perform source-aware inference at test time.

All scans are first processed by lung region extraction to suppress excessive irrelevant dark background around the body region. In addition, when the slice number exceeds 150, we discard the first 15% and the last 15% of slices to reduce unstable peripheral slices and excessive redundancy. After preprocessing, two stage-specific canonicalization strategies are adopted. For the 3D branch, each scan is converted to a volume of size $128 \times 256 \times 256$. For the 2D branch, each scan is canonicalized to $24 \times 448 \times 448$.

Our framework contains four trainable models. The first is a lung-aware 3D classifier in Stage 1, which directly predicts COVID/Non-COVID from canonicalized 3D CT volumes. The second is the Stage 2a model, which fine-tunes a pretrained MedSigLIP encoder by slice-wise representation and probability learning. The third is the Stage 2b model, which reuses the MedSigLIP encoder from Stage 2a, discards its original classification head, and introduces two Transformer encoder blocks for inter-slice context modeling. The fourth is a source classifier in Stage 3, which predicts the source identity of each scan and enables source-aware expert routing.

At inference time, the final prediction is determined according to the predicted source. Since the Stage 1 3D expert achieves perfect accuracy on source 0 in our validation analysis, scans predicted as source 0 are classified by the Stage 1 expert alone. For scans predicted as source 1/2/3, the predictions from Stage 1 and Stage 2 are combined by

expert voting and fusion. Moreover, multiple model variants are trained within each stage, and their predictions are aggregated by voting to further improve robustness.

2.2. Stage 1: Lung-Aware 3D Training for COVID-19 Classification

Stage 1 is designed to learn a robust volumetric expert from both raw CT scans and lung-extracted CT scans, following the line of research established by prior CMC-based methods [6–9]. After preprocessing and canonicalization, each scan is represented as a 3D volume $V \in \mathbb{R}^{128 \times 256 \times 256}$. To improve robustness against source-dependent background variation, we construct a mixed training set that contains both canonicalized original volumes and canonicalized lung-extracted volumes.

Given an input volume V , a 3D ResNet-style backbone [24] extracts a volumetric representation, which is then passed to a binary classification head for COVID/Non-COVID prediction. The output logit is denoted by $\mathbf{z}_{3D} \in \mathbb{R}^2$, and the corresponding probability is computed by softmax. The Stage 1 objective is standard cross-entropy:

$$\mathcal{L}_{3D} = - \sum_{c=0}^1 \mathbb{1}(y = c) \log p_{3D}(y = c | V). \quad (1)$$

During training, scan-level augmentation is applied to the 3D volumes, including cropping, resizing, and random rotation. Importantly, the same augmentation parameters are consistently applied to all slices within the same CT scan, while different scans use different random parameters. During validation, only deterministic resizing/rescaling is used. The optimized Stage 1 model serves not only as a strong 3D COVID-19 expert, but also as the feature backbone of the source classifier in Stage 3.

2.3. Stage 2a: Slice-Wise Representation and Probability Learning

Stage 2a adapts a pretrained MedSigLIP encoder to the COVID-19 CT task in a memory-efficient slice-wise manner. Each scan is first canonicalized to $24 \times 448 \times 448$. During training, instead of using all 24 slices at once, we randomly sample a contiguous 12-slice subsequence from the scan, denoted by $\tilde{U} = \{u_\tau, u_{\tau+1}, \dots, u_{\tau+11}\}$, where each slice $u_t \in \mathbb{R}^{448 \times 448}$.

Each sampled slice is independently fed into the pretrained MedSigLIP image encoder, followed by a binary classification head to obtain a slice-level probability. These 12 slice-level probabilities are then averaged to produce a scan-level prediction. Formally, if $p_t(y = c | u_t)$ denotes the predicted probability of class c for the t -th sampled slice, then the scan-level probability is

$$\bar{p}_{\text{slice}}(y = c | \tilde{U}) = \frac{1}{12} \sum_{t=1}^{12} p_t(y = c | u_t). \quad (2)$$

The corresponding training loss is

$$\mathcal{L}_{\text{slice}} = - \sum_{c=0}^1 \mathbb{1}(y = c) \log \bar{p}_{\text{slice}}(y = c | \tilde{U}). \quad (3)$$

This design allows Stage 2a to adapt the pretrained MedSigLIP encoder using scan-level supervision while avoiding excessive GPU memory consumption. At inference time, all 24 slices are used, and their probabilities are averaged in the same way to obtain the final Stage 2a prediction.

2.4. Stage 2b: Transformer-Based Inter-Slice Context Modeling

Although Stage 2a provides strong slice-level supervision, it does not explicitly model contextual dependency across adjacent slices. Therefore, in Stage 2b, we further build a sequence-level expert on top of the Stage 2a model.

Specifically, the MedSigLIP encoder trained in Stage 2a is reused as the visual backbone. Its original classification head is discarded, and most encoder layers are frozen, with only the last two layers kept trainable. Each of the 24 canonicalized slices is passed through this partially frozen encoder to obtain a sequence of slice embeddings. These embeddings are then fed into two Transformer encoder blocks to model inter-slice contextual relationships. The resulting contextualized slice features are aggregated into a scan-level representation, which is finally fed to a new binary classification head for COVID/Non-COVID prediction.

Let U denote the full 24-slice scan and let $p_{\text{ctx}}(y = c | U)$ denote the final scan-level probability predicted by this module. The Stage 2b objective is

$$\mathcal{L}_{\text{ctx}} = - \sum_{c=0}^1 \mathbb{1}(y = c) \log p_{\text{ctx}}(y = c | U). \quad (4)$$

Only the last two unfrozen MedSigLIP layers, the two Transformer encoder blocks, and the newly added classification head are updated in this stage. In this way, Stage 2b preserves the strong pretrained slice representation from Stage 2a while further introducing explicit cross-slice context modeling.

2.5. Stage 3: Source Discrimination and Source-Specific Expert Inference

The purpose of Stage 3 is to predict the hidden source identity of each scan and enable source-aware inference. To this end, we reuse the 3D backbone trained in Stage 1 and replace its binary classification head with a new four-class source classification head. The Stage 1 3D backbone is kept fixed and only the source classification head is trained. The resulting model predicts the source label $s \in \{0, 1, 2, 3\}$ for each scan.

Table 1. Official dataset split.

Split	Class	S0	S1	S2	S3	Total
Train	COVID	175	175	39	175	564
Train	Non-COVID	165	165	165	165	660
Val	COVID	43	43	0	42	128
Val	Non-COVID	45	45	45	45	180
Test	-	-	-	-	-	1488

Because the official validation split of source 2 contains no positive scans, we additionally include the 39 positive training scans from source 2 in source-aware validation analysis and model selection. After training, the source classifier is applied to the test set to estimate source identities.

At test time, source-aware expert inference is performed according to the predicted source. If a scan is predicted as source 0, the final label is directly determined by the Stage 1 3D expert, since this expert achieves perfect accuracy on source 0 in our validation experiments. If a scan is predicted as source 1/2/3, the predictions from Stage 1, Stage 2a, and Stage 2b are integrated by expert voting. Denoting the corresponding step-level voted predictions by $\tilde{y}^{(1)}$, $\tilde{y}^{(2a)}$, and $\tilde{y}^{(2b)}$, the final prediction can be written as

$$\hat{y} = \text{Vote}(\tilde{y}^{(1)}, \tilde{y}^{(2a)}, \tilde{y}^{(2b)}). \quad (5)$$

In practice, each stage contains multiple model variants with slightly different data processing settings but comparable performance, and their outputs are first aggregated within each step before cross-expert fusion. This hierarchical voting strategy improves robustness and helps stabilize prediction under source heterogeneity and source-specific data imbalance.

3. Datasets and Experiments

3.1. Datasets

The Multi-Source COVID-19 Detection Challenge provides a multi-institutional chest CT dataset collected from four different sources. The official split is summarized in Table 1. The training and validation sets contain binary labels (*COVID* vs. *Non-COVID*), whereas the test set contains 1488 unlabeled scans. A major challenge of this benchmark is that the data are highly heterogeneous across sources, not only in acquisition and appearance, but also in class composition and source-specific sample balance.

However, we found that directly using the official split is suboptimal for reliable model development and source-aware evaluation. Therefore, we performed three practical corrections.

First, since the official validation split of Source 2 contains no positive COVID cases, source-specific validation on this source is ill-posed. To alleviate this issue, we addi-

Table 2. Revised train/val statistics used in our experiments.

Split	Class	S0	S1	S2	S3	Total
Train	COVID	175	175	39	175	564
Train	Non-COVID	230	165	165	165	725
Val	COVID	43	43	39	42	167
Val	Non-COVID	45	45	45	45	180

tionally include the 39 positive Source 2 training scans in validation-oriented source analysis and model selection.

Second, for the Source 0 non-COVID training data, the official `ct_scan_8` entry was found to contain multiple folders, each representing an individual CT sample. Based on a folder-level inspection, the number of effective Source 0 non-COVID training scans was initially corrected from 165 to 231. Since `ct_scan_0` was confirmed to be absent, this number was subsequently adjusted to 230.

Third, since the challenge does not provide source labels for the test set, we estimate test-source identities using the Stage 3 source classifier. The raw predicted number of Source 0 test scans is 549, but because `ct_scan_492` also contains multiple CT samples and introduces ambiguity, we discard `ct_scan_492` and finally use 548 Source 0 test scans. The final predicted test-source distribution is 548/314/245/380 for Source 0/1/2/3, respectively, resulting in 1487 valid test scans used in our source-aware inference pipeline.

The corrected dataset statistics used in our experiments are summarized in Table 2.

3.2. Experiments

We evaluate each stage of the proposed framework separately and report the best-performing configurations. Since the challenge emphasizes robustness across heterogeneous sources, we mainly focus on macro-F1, while also reporting accuracy (ACC) and area under the ROC curve (AUC) when available.

3.2.1. Stage 1: Lung-Aware 3D Classification

Stage 1 directly trains a 3D COVID classifier on canonicalized volumetric CT scans. We compare several input settings, including original CT volumes, lung-extracted CT volumes, and their combination, with or without additional rotation-based augmentation. Table 3 summarizes the results.

As shown in Table 3, the best Stage 1 performance is obtained by combining *Orig* and *Lung*, which achieves the highest accuracy (**0.9712**) and macro-F1 (**0.9711**). This result indicates that the original scans and lung-focused scans capture complementary cues, and that their combination is more effective than either input alone. Notably, Stage 1 reaches a perfect score on Source 0, providing strong justification for using the Stage 1 expert alone on Source 0 in the final source-aware inference framework.

3.2.2. Stage 2a: Slice-Wise Representation and Probability Learning

Stage 2a adapts a pretrained MedSigLIP encoder via slice-wise probability learning. We evaluate several input construction strategies, including contiguous random depth sampling from canonicalized $24 \times 448 \times 448$ scans, contiguous random depth sampling from $128 \times 256 \times 256$ scans, and a depth-random-sampling variant applied to the $24 \times 448 \times 448$ setting. The quantitative results are reported in Table 4.

Overall, Stage 2a achieves strong performance, with the best macro-F1 reaching **0.9450** under contiguous random sampling and the highest AUC reaching **0.9864**. These results confirm that pretrained MedSigLIP can be effectively adapted to chest CT classification through slice-wise probability supervision.

3.2.3. Stage 2b: Transformer-Based Inter-Slice Context Modeling

Stage 2b further models inter-slice dependency on top of the pretrained MedSigLIP encoder from Stage 2a. We compare three settings: (1) training only the Transformer blocks and the new classification head, (2) jointly training the Transformer blocks, the classification head, and the last two MedSigLIP layers, and (3) directly flattening visual features followed by classification. The results are summarized in Table 5.

Among the three settings, *Flat + cls* delivers the best overall performance, achieving the highest macro-F1 (**0.9582**) and accuracy (**0.9597**). This result suggests that the pretrained MedSigLIP encoder already produces sufficiently discriminative slice representations, such that a lightweight classifier is enough to obtain strong classification performance. In contrast, *Trans + last2*, which additionally trains the Transformer encoder, the last two MedSigLIP layers, and the newly introduced classification head, achieves the highest AUC (**0.9854**), indicating improved ranking ability.

3.2.4. Stage 3: Source Classification

Stage 3 predicts the source identity of each scan for source-aware expert routing. The source classifier is built on top of the Stage 1 3D backbone and evaluated on the validation split with the additional Source 2 positive samples described above. The final Stage 3 source classifier achieves an ACC of 0.9107 and an F1 score of 0.9114.

These results indicate that the source classifier can provide sufficiently reliable source predictions for downstream source-aware expert inference. Combined with the observation that Stage 1 achieves perfect performance on Source 0, this makes it possible to route Source 0 scans directly to the 3D expert, while using multi-expert fusion for Source 1/2/3.

Table 3. Stage 1 results under different input configurations. *Lung* denotes the lung-extracted CT dataset, *Orig* denotes the original CT dataset, and *Rot* denotes random rotation augmentation. S0–S3 denote source-wise F1 scores on the four sources.

Setting	ACC	Macro-F1	AUC	S0	S1	S2	S3
Lung	0.9683	0.9682	0.9829	0.9886	0.9545	0.9523	0.9769
Lung + Rot	0.9568	0.9567	0.9803	1.0000	0.9204	0.9519	0.9540
Orig + Lung	0.9712	0.9711	0.9791	1.0000	0.9545	0.9642	0.9654
Orig	0.9625	0.9625	0.9776	0.9773	0.9773	0.9152	0.9770

Table 4. Stage 2a results using Orig + Lung inputs. “CRS” denotes contiguous random sampling and “DRS” denotes depth-random sampling.

Setting	ACC	Macro-F1	AUC
CRS (24×448×448)	0.9481	0.9450	0.9864
CRS (128×256×256)	0.9481	0.9425	0.9812
DRS (24×448×448)	0.9452	0.9440	0.9821

Table 5. Stage 2b results.

Setting	Macro-F1	ACC	AUC
Trans-only	0.9511	0.9539	0.9837
Trans + last2	0.9516	0.9539	0.9854
Flat + cls	0.9582	0.9597	0.9847

4. Conclusion

In this work, we presented a three-stage source-aware multi-expert framework for robust multi-source COVID-19 CT classification. Instead of relying on a single unified classifier, our method explicitly addresses the key challenges of this benchmark, including strong inter-source heterogeneity, source imbalance, source-specific validation difficulty, and hidden test-source identities. The proposed framework integrates a lung-aware 3D expert for volumetric modeling, two MedSigLIP-based 2D experts for slice-wise adaptation and inter-slice context modeling, and a source classifier for source-aware routing and expert fusion.

The experimental results validate the effectiveness of this design. Stage 1 provides the strongest overall performance and achieves perfect accuracy on Source 0, which supports source-specific expert allocation. Stage 2 further contributes complementary discriminative cues through pretrained 2D visual modeling and inter-slice refinement. Stage 3 enables reliable source prediction and makes source-aware inference feasible on the unlabeled test set. By combining multiple experts and aggregating their outputs through hierarchical voting, our framework

achieves robust and stable performance under challenging multi-source conditions.

Overall, our results suggest that multi-source COVID-19 CT detection should be addressed not only as a binary classification problem, but also as a source-aware domain-robust inference problem. We believe the proposed framework provides a practical and effective paradigm for building reliable medical imaging systems under real-world cross-institutional heterogeneity.

Acknowledgements. This work was supported by National Natural Science Foundation of China (No. 62576107), and the Shanghai Municipal Commission of Economy and Informatization, Corpus Construction for Large Language Models in Pediatric Respiratory Diseases (No.2024-GZL-RGZN-01013, and the Science and Technology Commission of Shanghai Municipality (No.24511104200), and 2025 National Major Science and Technology Project - Noncommunicable Chronic Diseases-National Science and Technology Major Project, Research on the Pathogenesis of Pancreatic Cancer and Novel Strategies for Precision Medicine (No.2025ZD0552303).

References

- [1] Anastasios Arsenos, Dimitrios Kollias, and Stefanos Kollias. A large imaging database and novel deep neural architecture for covid-19 diagnosis. In *2022 IEEE 14th Image, Video, and Multidimensional Signal Processing Workshop (IVMSP)*, pages 1–5. IEEE, 2022. 1
- [2] Anastasios Arsenos, Andjoli Davidhi, Dimitrios Kollias, Panos Prassopoulos, and Stefanos Kollias. Data-driven covid-19 detection through medical imaging. In *2023 IEEE International Conference on Acoustics, Speech, and Signal Processing Workshops (ICASSPW)*, pages 1–5. IEEE, 2023.
- [3] Jiawang Cao, Lulu Jiang, Junlin Hou, Longquan Jiang, Ruiwei Zhao, Weiya Shi, Fei Shan, and Rui Feng. Exploiting deep cross-slice features from ct images for multi-class pneumonia classification. In *2021 IEEE International Conference on Image Processing (ICIP)*, pages 205–209. IEEE, 2021.
- [4] Demetris Gerogiannis, Anastasios Arsenos, Dimitrios Kollias, Dimitris Nikitopoulos, and Stefanos Kollias. Covid-19 computer-aided diagnosis through ai-assisted ct imaging

- analysis: Deploying a medical ai system. In *2024 IEEE International Symposium on Biomedical Imaging (ISBI)*, pages 1–4. IEEE, 2024.
- [5] Hayden Gunraj, Ali Sabri, David Koff, and Alexander Wong. Covid-net ct-2: Enhanced deep neural networks for detection of covid-19 from chest ct images through bigger, more diverse learning. *Frontiers in Medicine*, 8:729287, 2022. 1
- [6] Junlin Hou, Jilan Xu, Rui Feng, Yuejie Zhang, Fei Shan, and Weiya Shi. Cmc-cov19d: Contrastive mixup classification for covid-19 diagnosis. In *Proceedings of the IEEE/CVF International Conference on Computer Vision*, pages 454–461, 2021. 3
- [7] Junlin Hou, Jilan Xu, Longquan Jiang, Shanshan Du, Rui Feng, Yuejie Zhang, Fei Shan, and Xiangyang Xue. Periphery-aware covid-19 diagnosis with contrastive representation enhancement. *Pattern Recognition*, 118:108005, 2021.
- [8] Junlin Hou, Jilan Xu, Nan Zhang, Yi Wang, Yuejie Zhang, Xiaobo Zhang, and Rui Feng. Cmc.v2: Towards more accurate covid-19 detection with discriminative video priors. In *European Conference on Computer Vision*, pages 485–499. Springer, 2022.
- [9] Junlin Hou, Jilan Xu, Nan Zhang, Yuejie Zhang, Xiaobo Zhang, and Rui Feng. Boosting covid-19 severity detection with infection-aware contrastive mixup classification. In *European Conference on Computer Vision*, pages 537–551. Springer, 2022. 3
- [10] Dimitrios Kollias, Athanasios Tagaris, Andreas Stafylopatis, Stefanos Kollias, and Georgios Tagaris. Deep neural architectures for prediction in healthcare. *Complex & Intelligent Systems*, 4(2):119–131, 2018. 1
- [11] Dimitrios Kollias, N Bouas, Y Vlaxos, V Brillakis, M Seferis, Ilianna Kollia, Levon Sukissian, James Wingate, and S Kollias. Deep transparent prediction through latent representation analysis. *arXiv preprint arXiv:2009.07044*, 2020.
- [12] Dimitris Kollias, Y Vlaxos, M Seferis, Ilianna Kollia, Levon Sukissian, James Wingate, and S Kollias. Transparent adaptation in deep medical image diagnosis. In *International Workshop on the Foundations of Trustworthy AI Integrating Learning, Optimization and Reasoning*, pages 251–267. Springer, 2020.
- [13] Dimitrios Kollias, Anastasios Arsenos, Levon Soukissian, and Stefanos Kollias. Mia-cov19d: Covid-19 detection through 3-d chest ct image analysis. In *Proceedings of the IEEE/CVF International Conference on Computer Vision*, pages 537–544, 2021.
- [14] Dimitrios Kollias, Anastasios Arsenos, and Stefanos Kollias. Ai-mia: Covid-19 detection and severity analysis through medical imaging. In *European conference on computer vision*, pages 677–690. Springer, 2022.
- [15] Dimitrios Kollias, Anastasios Arsenos, and Stefanos Kollias. Ai-enabled analysis of 3-d ct scans for diagnosis of covid-19 & its severity. In *2023 IEEE International Conference on Acoustics, Speech, and Signal Processing Workshops (ICASSPW)*, pages 1–5. IEEE, 2023.
- [16] Dimitrios Kollias, Anastasios Arsenos, and Stefanos Kollias. A deep neural architecture for harmonizing 3-d input data analysis and decision making in medical imaging. *Neuro-computing*, 542:126244, 2023.
- [17] Dimitrios Kollias, Anastasios Arsenos, and Stefanos Kollias. Domain adaptation explainability & fairness in ai for medical image analysis: Diagnosis of covid-19 based on 3-d chest ct-scans. In *Proceedings of the IEEE/CVF Conference on Computer Vision and Pattern Recognition*, pages 4907–4914, 2024.
- [18] Dimitrios Kollias, Anastasios Arsenos, James Wingate, and Stefanos Kollias. Sam2clip2sam: Vision language model for segmentation of 3d ct scans for covid-19 detection. *arXiv preprint arXiv:2407.15728*, 2024.
- [19] Dimitrios Kollias, Anastasios Arsenos, and Stefanos Kollias. Pharos-afe-aimi: Multi-source & fair disease diagnosis. In *Proceedings of the IEEE/CVF International Conference on Computer Vision*, pages 7265–7273, 2025.
- [20] David Krueger, Ethan Caballero, Joern-Henrik Jacobsen, Amy Zhang, Jonathan Binas, Dinghuai Zhang, Remi Le Priol, and Aaron Courville. Out-of-distribution generalization via risk extrapolation (rex). In *International conference on machine learning*, pages 5815–5826. PMLR, 2021.
- [21] Qingqiu Li, Runtian Yuan, Junlin Hou, Jilan Xu, Yuejie Zhang, Rui Feng, and Hao Chen. Advancing covid-19 detection in 3d ct scans. In *Proceedings of the IEEE/CVF Conference on Computer Vision and Pattern Recognition*, pages 5149–5156, 2024.
- [22] Qingqiu Li, Runtian Yuan, Junlin Hou, Jilan Xu, Yuejie Zhang, Rui Feng, and Hao Chen. Advancing lung disease diagnosis in 3d ct scans. In *Proceedings of the IEEE/CVF International Conference on Computer Vision*, pages 7377–7382, 2025. 1
- [23] Andrew Sellergren, Sahar Kazemzadeh, Tiam Jaroensri, Atilla Kiraly, Madeleine Traverse, Timo Kohlberger, Shawn Xu, Fayaz Jamil, Cían Hughes, Charles Lau, et al. Medgemma technical report. *arXiv preprint arXiv:2507.05201*, 2025. 1
- [24] Ashish Vaswani, Noam Shazeer, Niki Parmar, Jakob Uszkoreit, Llion Jones, Aidan N Gomez, Łukasz Kaiser, and Illia Polosukhin. Attention is all you need. *Advances in neural information processing systems*, 30, 2017. 1, 3
- [25] Zifeng Wang, Zhenbang Wu, Dinesh Agarwal, and Jimeng Sun. Medclip: Contrastive learning from unpaired medical images and text. In *Proceedings of the 2022 Conference on Empirical Methods in Natural Language Processing*, pages 3876–3887, 2022. 1
- [26] Runtian Yuan, Qingqiu Li, Junlin Hou, Jilan Xu, Yuejie Zhang, Rui Feng, and Hao Chen. Domain adaptation using pseudo labels for covid-19 detection. In *Proceedings of the IEEE/CVF Conference on Computer Vision and Pattern Recognition*, pages 5141–5148, 2024.
- [27] Runtian Yuan, Qingqiu Li, Junlin Hou, Jilan Xu, Yuejie Zhang, Rui Feng, and Hao Chen. Multi-source covid-19 detection via variance risk extrapolation. In *Proceedings of the IEEE/CVF International Conference on Computer Vision*, pages 7304–7311, 2025.
- [28] Hongyi Zhang, Moustapha Cisse, Yann N Dauphin, and David Lopez-Paz. mixup: Beyond empirical risk minimization. *arXiv preprint arXiv:1710.09412*, 2017. 1